Experimental analysis of influence of error on super-resolution optical inspection using standing wave illumination

Ryota Kudo[1,#], Shin Usuki[2], Satoru Takahashi[1] and Kiyoshi Takamasu[1]

1 Department of Precision Engineering, The University of Tokyo, Hongo 7-3-1, Bunkyo-ku, Tokyo, 113-8656, Japan

2 Division of Global Research Leaders, Shizuoka University, Johoku 3-5-1, Naka-Ku, Hamamatsu 432-8561, Japan

Corresponding Author / E-mail: honc@nanolab.t.u-tokyo.ac.jp, TEL: +81-3-5841-6472, FAX: +81-3-5841-6472

KEYWORDS : Standing wave illumination, Image reconstruction, Super-resolution

Microfabricated structures such as semiconductors and MEMS keep shrinking as nanotechnology advances. Demand that measures microfabricated structures has risen. The optics and electron beam have been mainly used for that purpose, but the resolving power of the optics is limited by the Rayleigh limit and it is generally low for defects at sub-wavelength geometries, while the scanning electron microscope needs vacuum and induces contamination in measurement. In order to find a solution to these problems, we propose the novel optical inspecting method for the microfabricated structure using standing wave shift. This method is based on a super-resolution algorithm in which the inspection system's resolution exceeds the Rayleigh limit by shifting standing wave with the piezoelectric actuator. Until now, resolution which is beyond Rayleigh limit is theoretically studied and experimentally bought to realization. It is necessary to investigate the influence that various experimental error factors gives, and to reflect it in the calibration when actual application is constructed. The error factor includes the phase, the pitch, and the shift step size of the standing wave. It is the most difficult to identify the phase accurately, and greatly influences the resolution result. So, the standing wave phase was focused as experimental error factor. The influence of the phase difference between actual experimental standing wave and standing wave computationally set was investigated based on the computer simulation and the experimental data. The following findings were obtained as a result. The phase difference of the standing wave shifts the periodical structure of the super-resolution image. The larger the phase difference of the standing wave is the more greatly the periodical structure of the sample shifts. It was confirmed that the 200 nm interval periodical structure of the sample was able to be detected though the super-resolution image shifted horizontally under the condition that Rayleigh limit is 590 nm.

Manuscript received: January XX, 2011 / Accepted: January XX, 2011

NOMENCLATURE

SWI = standing wave illumination

1. Introduction

According to the ITRS roadmap [1], a next-generation semiconductor defect inspection system is urgently demanded, and the challenges for defect detection increase exponentially with shrinking design, such as sub-100-nm nodes. One of the key areas where improvement is needed is defect detection of semiconductor wafers [4]. Defects in the wafers include random defects like killer particles, clustered defects, scratch defects and so on. These defects deteriorate electrical chip performance and process yield in the semiconductor manufacturing process. Especially, improved inspection of patterned wafers is a necessity for the next generation of semiconductors.

Optical methods and electron beams are conventionally used for semiconductor wafer inspection [5]. However, with the continuous miniaturization of interconnects, optical inspection becomes less useful because of its diffraction limit. On the other hand, electron beams lack utility for wider wafer inspection because of their low

throughput property. We think optical inspection has greater potential than SEM inspection for inspection under the less-than-50nm design rule and 300mm wafers because optical inspection is non-destructive and has high throughput. So, we focused our attention on optical inspection. In optical wafer inspection, resolution and defect detection beyond the Rayleigh limit are now required due to the acceleration of pattern miniaturization and development of advanced semiconductor devices [6].

One of the solutions to challenges in semiconductor optical inspection is the use of shorter wavelengths, which has been studied as a countermeasure against device miniaturization. However, as the shortening of wavelength is too limited to keep up with the challenges, we have developed a super-resolution inspection technique. Namely, when a pattern is miniaturized and made dense, light reflected from the wafer becomes weak, and the captured image becomes dark with low contrast; hence, a high-sensitivity method that can obtain a lot of optical information must be developed [7]. Our super-resolution inspection technique combines a SWI shift method with dark-field imaging technology to deliver optimal sensitivity for critical defect detection at sub-100-nm nodes and beyond, without compromising throughput. The SWI shift method enables the optical resolution of patterns that the conventional method cannot achieve. Nano-scale shifts of illumination and super-resolution post-processing are keys to achieving the resolution enhancement and higher sensitivity for defect detection.

In this paper, indispensable investigation of what influence is brought to the super-resolution result by effect of error for construction of an actual application, is carried out computationally and experimentally. The phase of the SWI that brought the influences to the resolution result most when experiment is carried out among various errors was investigated. It was confirmed to be able to detect the periodical structure even if error of phase difference existed.,

2. Methodology

2.1 Standing wave illumination shift and scattered light mo dulation

A schematic diagram of the SWI shift and the scattered light modulation is shown in Fig. 1. The SWI is generated by 2-beam interference. The SWI is scattered by the sample surface, and the scattered light is focused on the CCD imaging surface through the imaging lens. The SWI is shifted on a nanoscale by the phase difference between the 2 beams in the illumination (Fig. 1 (a)). Then, the scattered light is modulated by the shift of the SWI (Fig. 1 (b)). A super-resolution image of scattering efficiency can be calculated from multiple images by the super-resolution image reconstruction algorithm.

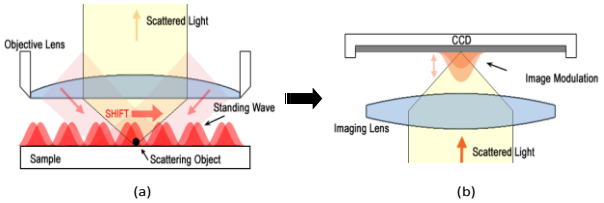

Fig. 1 Schematic diagram of the SWI shift and the scattered light modulation

2.2 Super-resolution image reconstruction algorithm for post processing

A block diagram of the super-resolution post-processing is shown in the Fig. 2. First, the sample is illuminated with SWI, and multiple images are experimentally observed by the SWI shift. Then, calculated images are computationally obtained based on Fourier optics. The error between the observed images and the calculated images is approximately fed back to the assumed sample to obtain a reconstructed sample. The image reconstruction is iteratively calculated with successive approximation until the error converges. The nanoshifts of SWI that are modulated at about a half-wavelength scale include high-frequency spatial information, and this causes change to the scattered light images. We expect to achieve super resolution by feeding back the errors in scattered light images into sample distribution and reconstructing the sample distribution with successive approximation.

Fig. 3 shows the schematics of super resolution. When two point samples to be observed are close enough (shown as two blue dots), the two points cannot be distinguished in the observed image. Then, the sample is illuminated by the SWI, and multiple modulated scattered light images are obtained. These obtained images are post-processed; then the two point samples are clearly resolved as shown in the lower right image. Thus, a super resolution is achieved.

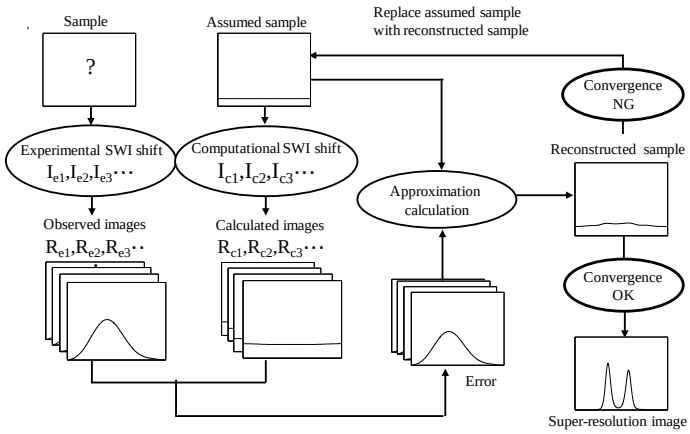

Fig. 2 Block diagram of the super-resolution post-processing

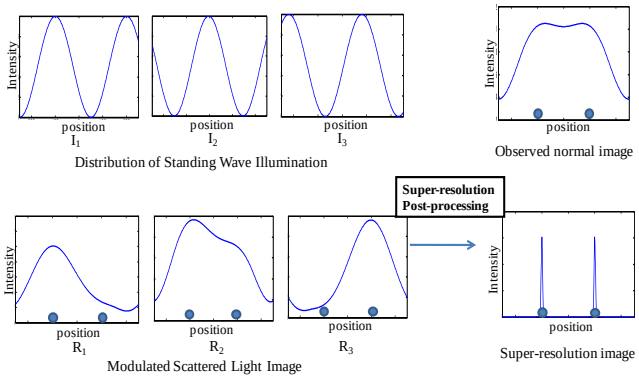

Fig. 3 Example that 2 point sample is resolved by super-resolution

3. Simulation based analysis of influence of error

There are a phase, a pitch, and a shift step size, etc. as an error factor in the SWI. It is easy to identify an accurate value comparatively for the pitch and the shift step size when

experimenting. On the other hand, it is difficult to identify SWI phase accurately and greatly influences the resolution result. Then, the phase difference of the SWI that influences it most on super-resolution experiment is investigated. To investigate what influence of the resolution characteristic is caused when phase difference existed between the SWI that actually illuminated the sample (experimental SWI in Fig. 2) and the SWI set by the super-resolution post-processing (computational SWI in Fig. 2), the computer simulation was carried out. Phase difference between Computational SWI and experimental SWI is shown in Fig. 4. Even if SWI is shifted, phase difference is constant. In other words, phase difference between I_{e1} and I_{c1} and phase difference between I_{e2} and I_{c2} are corresponding even if I_{e1} and I_{c1} shift respectively and they become I_{e2} and I_{c2}. Simulation setup is shown in Table 1. This simulation conditions were set according to the specification of the experimental equipment described later for the comparison with the experiment. A periodic structure to assume the structure of the semiconductor was adopted in the object sample as a survey of the first stage. The structure that the 200 nm L&S pattern was assumed and constant scattered efficiency existed in the line edge of every 200 nm is set (Fig. 5 (a)). Fig. 5 (b) is the normal microscopic image of uniform illumination: a bandwidth-limited image by *NA*. It is confirmed that the structure of the sample is not resolved in Fig. 5 (b). Fig. 6 shows the result of processing super-resolution to the sample of Fig. 5 (a) in consideration of the phase difference of the SWI. Fig. 6 (b) is a result when phase difference doesn't exist and Fig. 6 (c) and (d) are cases where the phase difference of $\pi/2$ and π exists respectively. Fig. 6 (b) shows the resolution result the peak of the scattered light intensity being reconstructed by a position almost corresponding to a true structure of the sample (Fig. 6 (a)). It was shown that a structural resolution at 200 nm intervals was possible under the condition of Table 1. On the other hand, Fig. 6(c) and (d) shift to the result of Fig. 6 (b) by 50 nm and 100 nm respectively though are equal to Fig. 6 (b) the pitch of the periodical structure reconstructed. When 200 nm interval of the periodical structure of the sample is considered as 2π, it can be said that the gap of $\pi/2$ and π was caused in the resolution result. It was confirmed that the periodical structure of the sample reconstructed corresponding to the phase difference of the SWI shifted.

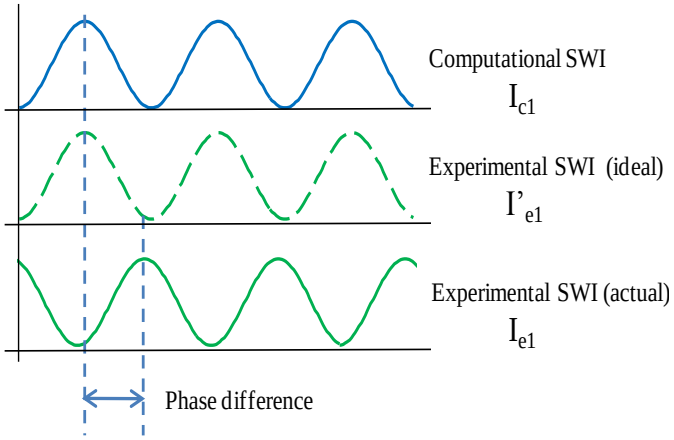

Fig. 4 Phase difference between computational SWI and experimental SWI.

Table 1 Simulation setup

Wavelength of source	532 nm
Pitch of SWI	270 nm
Objective lens	*NA* 0.55
Rayleigh limit	590 nm
Shift step size	8.2 nm
Shift times	32
Iteration loop times	2

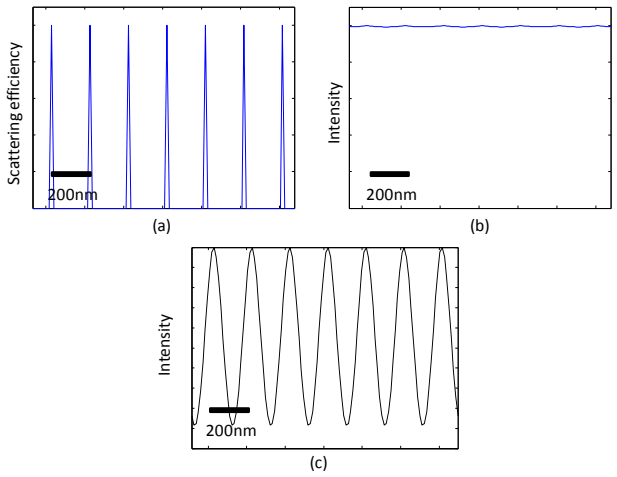

Fig. 5 (a) Employed sample of 200 nm interval periodical structure, (b) Normal imaging of *NA* 0.55, (c) Super-resolution image

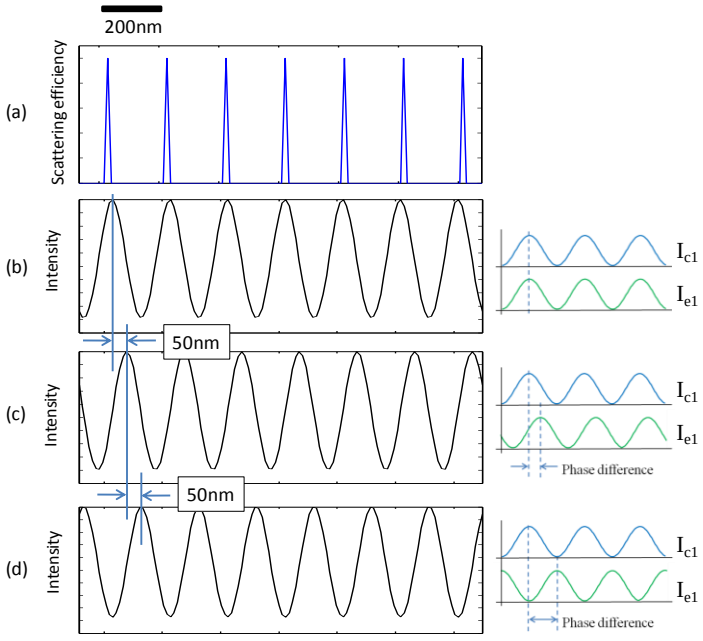

Fig. 6 Shift of super-resolution image with phase difference (a) Employed sample distribution. Super-resolution image with SWI phase difference of (b) 0, (c) $\pi/2$, (d) π

4. Experimental equipment for super-resolution

Experimental equipment was constructed for the super-resolution experiment. Fig. 7 and Fig. 8 show a schematic diagram of the experimental equipment. The following features must be attained by experimental super-resolution equipment. First, two orthogonal SWIs

must be generated on the sample. This is achieved by the optical system of 4 incident light directions as shown in Fig. 7. Second, each SWI must be able to shift on a nanoscale. PZTs attached to mirror 5 and 6 in Fig. 7 give a phase difference between the 2 beams and enable this feature. Dark-field scattered light detection is also a necessary feature for sensitive detection of defects. This is achieved by an optical system by which incident light enters from outside the objective lens (Fig. 8). A photograph of the experimental apparatus is shown in Fig. 9. Table 2 shows the parameters of the equipment. An objective lens of comparatively low *NA* which allows us to clearly verify the proposed method is used.

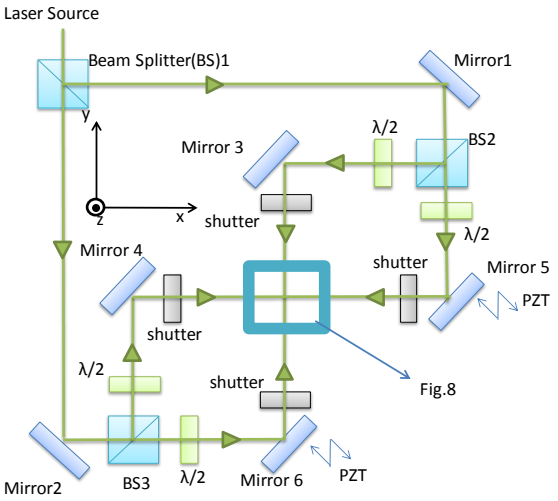

Fig. 7 Schematic diagram of optical system of 4 incident light directions for 2D super-resolution (top view)

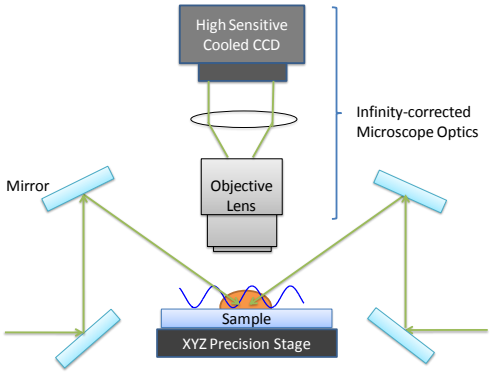

Fig. 8 Schematic diagram of dark-field scattered light detection system (side view)

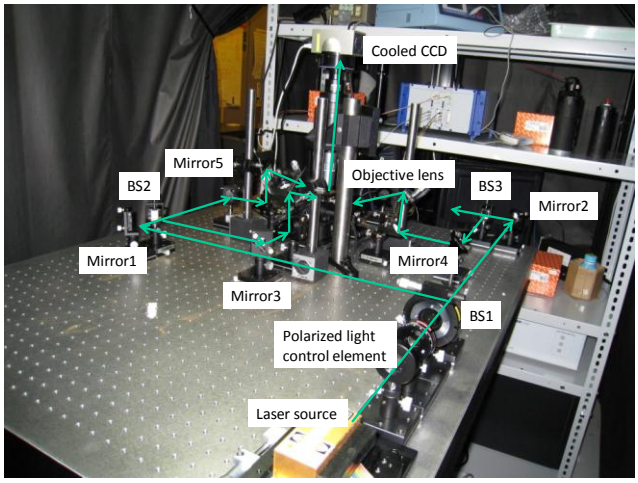

Fig. 9 Photograph of experimental equipment

Table 2 Parameters of the experimental apparatus

Wavelength of source	532 nm
Pitch of SWI	266 nm~350 nm
Objective lens	*NA* 0.55 ×100
Rayleigh limit	590 nm
Resolution of SWI shift	0.8 nm
CCD pixel size	8.3 μm × 8.3 μm

5. Experimental analysis of influence of error

5.1 Basic super-resolution experiment

A sample which has a 200 nm L&S pattern, 3 attached foreign particles and carbon contamination [8] was employed for super-resolution experiment. Fig. 10(a) shows SEM images of the sample. A schematic diagram of the sample is shown in Fig. 10(b). Fig. 10(c) shows images of the sample observed by the equipment when incident light entered from the left. The 200nm L&S pattern in this image is not resolved, and the positions of attached foreign particles and carbon contamination are unclear due to low *NA*. Then a super-resolution experiment was carried out on the sample. The experimental setup is defined in Table 3.

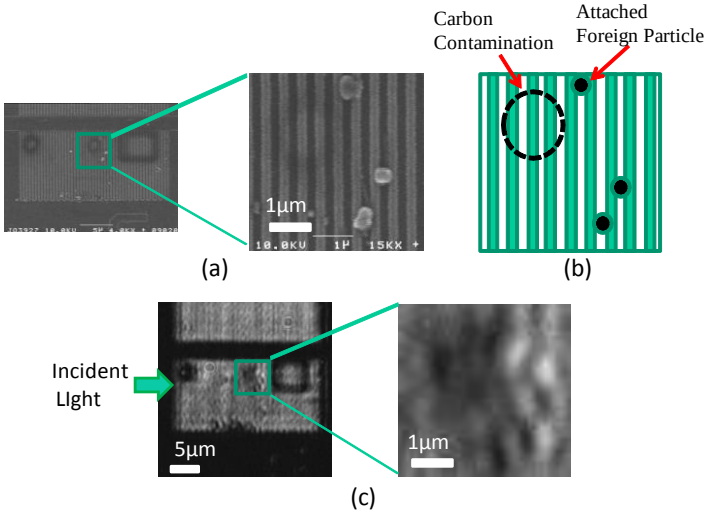

Fig. 10 Employed sample (a) SEM image, (b) The schematic diagram, (c) Normal imaging of *NA* 0.55

Table 3 Experimental setup

Pitch of SWI	270 nm
Shift step size	8.3 nm
Shift times	*x* 32 *y* 32
Iteration loop times	2

super-resolution post-processing was carried out. The super-resolution image of the sample is shown in Fig. 11(b). The structure, which was not resolved in the image before super-resolution post-processing (Fig. 11(a)), is resolved in Fig. 11(b). In Fig. 11(b), the edges of the 200 nm L&S pattern are clearly resolved, and positions of the attached foreign particles and carbon contamination become clearer under the condition that Rayleigh limit is 590 nm.

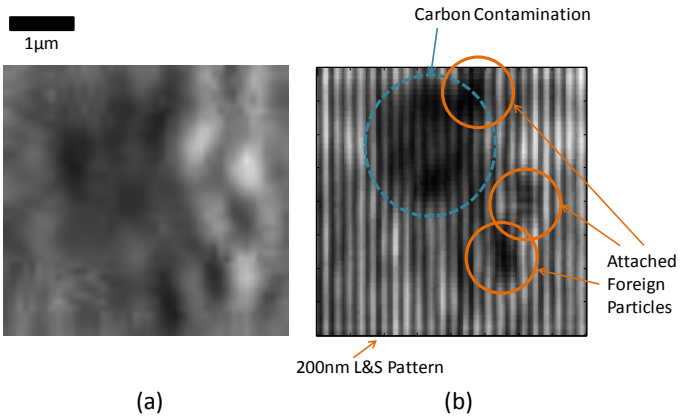

Fig. 11 Comparison between normal image and reconstructed super-resolution image (a) Normal imaging of *NA* 0.55, (b) Super-resolution image

5.2 Experimental analysis (error factor: phase of SWI)

The influence that the phase difference that existed between the SWI that actually illuminated the sample and the SWI set by the super-resolution post-processing exerted on the resolution characteristic was experimentally investigated. Fig. 12 shows the result of processing super-resolution to the sample of Fig. 10 in consideration of the phase difference of the SWI. The SWI phase in Fig. 12(a) is treated as a standard as follows though the phase of the SWI cannot be decided in high accuracy with the experimental equipment. Fig. 12(b) and (c) are cases where the phase difference of $\pi/2$ and π exists respectively against the SWI used to process Fig. 12(a). The one dimensional profile (Fig. 12(B)) was taken out of the same position of two dimensional super-resolution image (Fig. 12(A)). Fig. 13 shows the one that Fig. 12(B) was displayed to the vertical direction. The line edge at 200 nm intervals has been resolved in Fig. 13(a), (b), and (c). It seems that the reason why the resolution result doesn't necessarily become like the sine wave like the simulation is an influence by the noise such as the ununiformity of the scattered efficiency distribution of the sample, the speckle of the illumination, and the vibrations, etc. When the periodical structure of the reconstructed result is paid attention, Fig. 13(b) and (c) are the results of the shift to the result of Fig. 13(a) by 50 nm and 100 nm respectively. When 200 nm intervals of the periodical structure of the sample is considered as 2π, it can be said that the gap of $\pi/2$ and π was caused in the super-resolution image. It was confirmed experimentally that the periodical structure of the sample reconstructed corresponding to the phase difference of the SWI shifted. The phenomenon expected by the computer simulation was experimentally reproduced. It was confirmed that the detection of the periodical structure at 200 nm intervals was possible regardless of phase difference of SWI. It is necessary to know the phase of the SWI in high accuracy to match the periodical structure of the sample reconstructed to a true sample structure absolutely. It is difficult to identify the phase of the SWI in high accuracy in current super-resolution experimental equipment. The experimental equipment and the experimental maneuver that can identify the phase of the SWI in high accuracy will be developed in the future.

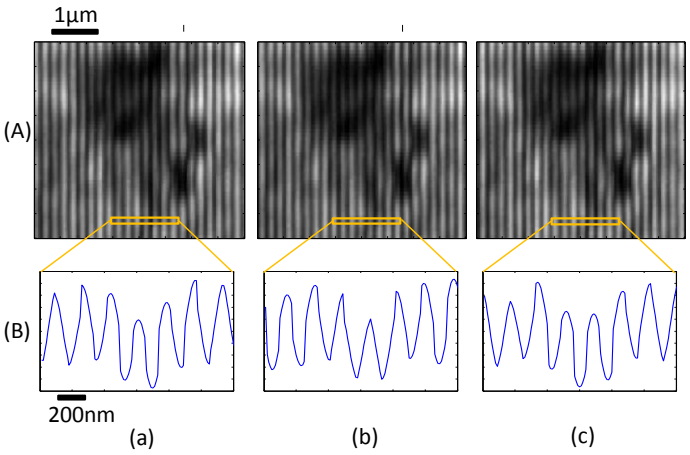

Fig. 12 Super-resolution images with SWI phase difference of (a) 0 (standard), (b) $\pi/2$, (c) π,
(A) Two dimensional super-resolution image, (B) One dimensional profile of super-resolution image,

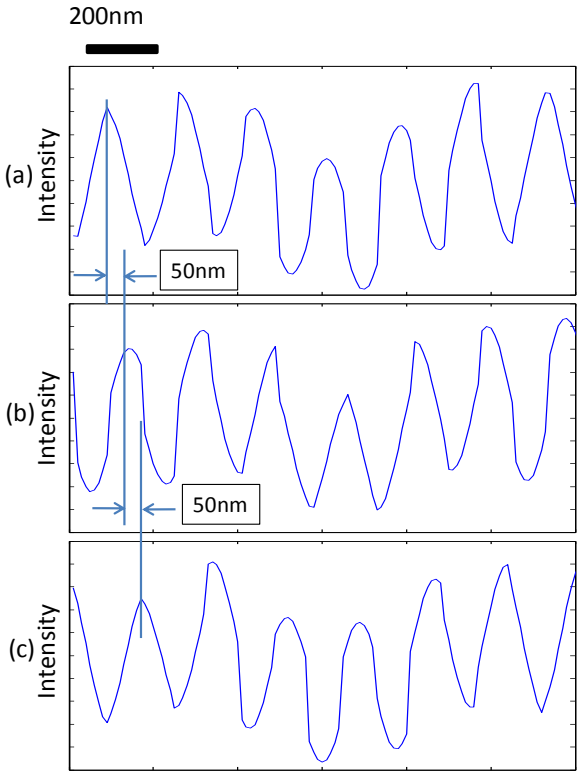

Fig. 13 Shift of super-resolution result, one dimensional profile of super-resolution result with SWI phase difference of (a) 0 (standard), (b) $\pi/2$, (c) π

6. Conclusions

It is necessary to investigate the influence that various experimental error factors gives, and to reflect it in the calibration when actual application that applies proposed super-resolution method is constructed. The error factors include the phase, the pitch, and the shift step size of the SWI. It is the most difficult to identify the phase accurately, and greatly influences the resolution result. So, the SWI phase was focused as experimental error factor. The influence of the phase difference between actual experimental

standing wave and standing wave computationally set was investigated based on the computer simulation and the experimental data. As the first stage, the sample that assumed the pattern of the semiconductor with the 200 nm periodical structure was adopted and it investigated.

By simulation based analysis of influence of phase difference, it was confirmed that the periodical structure of the sample reconstructed corresponding to the phase difference of the SWI shifted. The 200 nm pitch of the periodical structure can be detected regardless of phase difference of SWI under the condition that Rayleigh limit is 590 nm.

By experimental analysis of influence of phase difference, super-resolution image shifted corresponding to phase difference of the SWI as well as the analysis by the simulation. It was confirmed that the 200 nm intervals periodical structure of the sample was able to be detected though the super-resolution image shifted horizontally under the condition that Rayleigh limit is 590 nm.

The influence of the error will be investigated from both sides of the simulation and the experiment about samples that don't have periodical structure in the future.

ACKNOWLEDGEMENT

The author (One of the authors (Ryota Kudo)) was supported through the Global COE Program, “Global Center of Excellence for Mechanical Systems Innovation,” by the Ministry of Education, Culture, Sports, Science and Technology.

This work was partially supported by NEDO under the Industrial Technology Research Grant Program.

REFERENCES

1. "International Technology Roadmap for Semiconductors, Metrology (2008 update)", Semiconductor Industry Association
2. H. Nishioka, S. Takahashi, K. Takamasu, Proc. of IMEKO World Congress, 12, TC2, 2006.
3. S. Usuki, H. Nishioka, S. Takahashi, K. Takamasu, SPIE International Symposium on Optmechatronic Technologies 2005, (2005), pp60490C-1~60490C-11.
4. Mark A. Schulze, Martin A. Hunt, Edgar Voelkl, Joel D. Hickson, William Usry, Randall G. Smith, Robert Bryant and C. E. (Tommy) Thomas Jr., Proc. SPIE's Advanced Microelectronic Micromanufacturing, 27-28 February 2003
5. George W. Mulholland and Thomas A. Germer, Proc. the Government Microcircuits Applications and Critical Technologies (GOMACTech) Conference, March 31 to April 3, 2003
6. Kenji Watanabe, Shunji Maeda, Tomohiro Funakoshi and Yoko Miyazaki, Hitachi Review Vol. 54, No. 1, pp22-26, 2005
7. Volker Westphal and Stefan W. Hell, PHYSICAL REVIEW LETTERS, No.143903, 2005
8. A. E. Vladár and M.T.Postek, Microsc Microanal 11(Suppl2),2005